Supplementary text for the manuscript:

Self-sensing in *Bacillus subtilis* quorum-sensing systems

Tasneem Bareia, Shaul Pollak and Avigdor Eldar

School of Molecular Cell Biology and Biotechnology, Faculty of Life Sciences, Tel-Aviv University, Tel-Aviv, Israel

Contents

Supplementary Figures

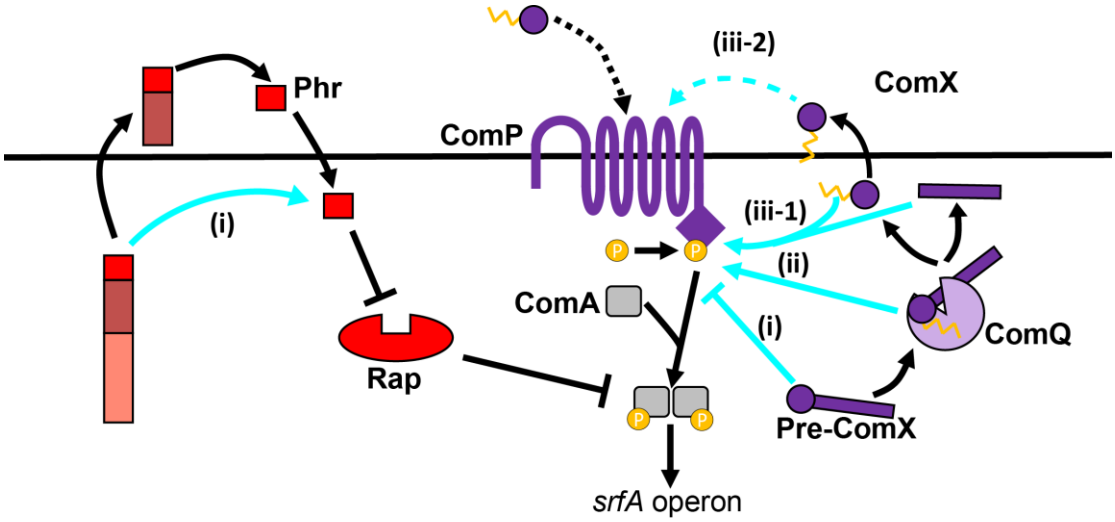

Rap-Phr system
i. Self-sensing (internal cleavage?)

ComQXP system
i. *comX* dependent over-reception
ii. *comQ* dependent over-reception
iii. (1) *comQX* dependent over-reception
(2) Self-sensing (membrane tethering?)

Supplementary Figure 1: Mechanism of *B. subtilis* quorum-sensing and several models for cell-autonomous effects. The ComX autoinducer is a product of post-translational cleavage and modification (yellow zig) of the Pre-ComX peptide by the ComQ enzyme. ComX binding to the ComP receptor kinase leads to phosphorylation of ComA. The Phr autoinducer results from multiple post-translational cleavages of the Pre-Phr peptide. Phr is imported back into the cell, where it interacts with the corresponding Rap to prevent it from repressing ComA. Several mechanisms for cell autonomous effects (either self-sensing or over-reception) are shown using cyan arrows and annotated at the bottom of the figure.

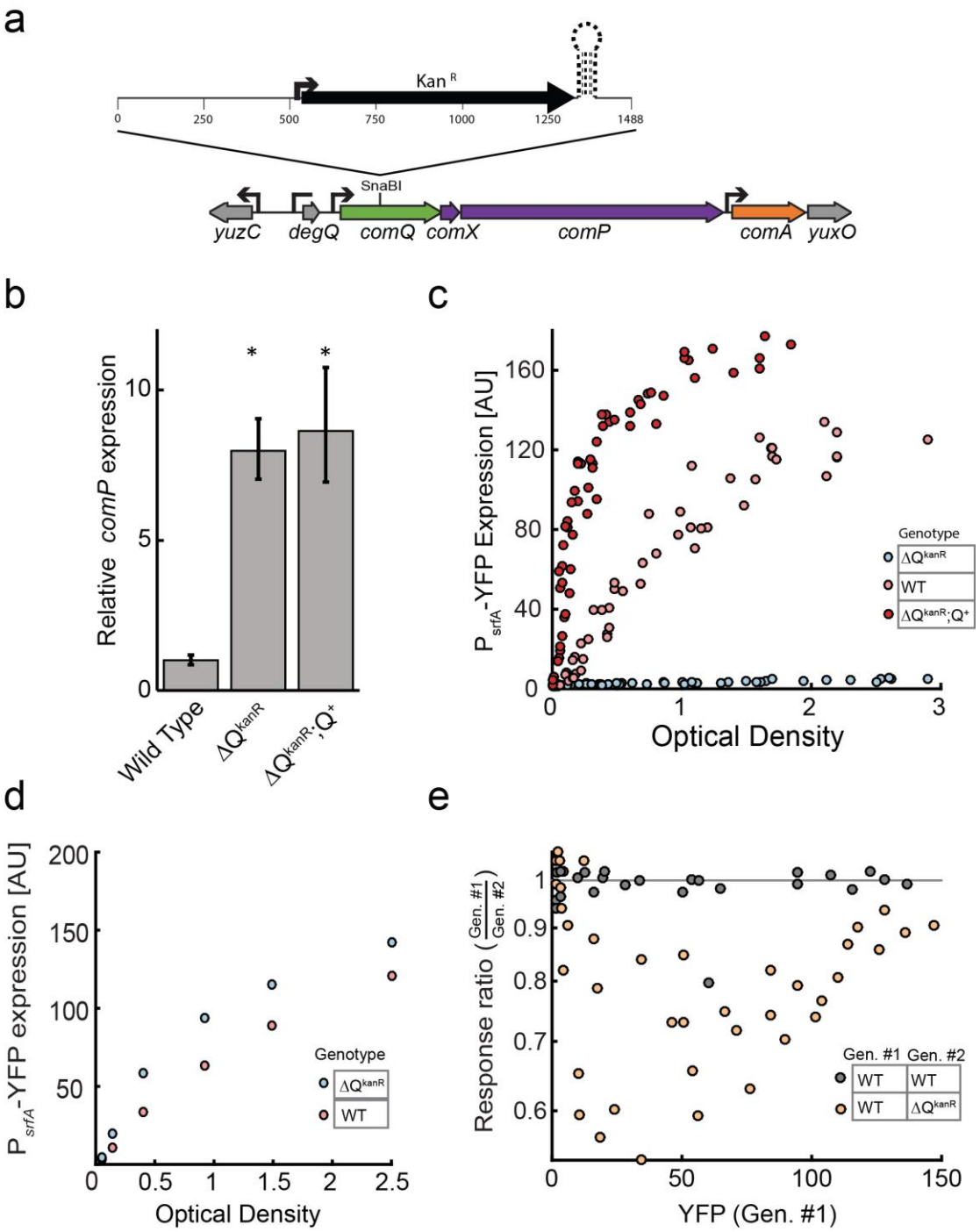

Supplementary Figure 2: The comQ::kanR (*ΔQ^{kanR}*) mutation renders the strain hyper-sensitive to ComX due to a polar over-expression effect on *comP*. (a) Schematic presentation of the *comQXP* operon and the *aphA3* kanamycin-resistance gene inserted into it. The directionality of the insertion has not been determined in the past and was determined here by sequencing. (b) *comP* transcript levels in the wild-type (normalized to 1), Δ*Q^{kanR}* and Δ*Q^{kanR};Q^{+}* strains. See methods for details. The two Δ*Q^{kanR}*-based strains exhibited significantly

different levels of *comP* expression as compared to the wild-type (n=3 for both comparisons, Tukey-Kramer corrected p-value<0.05 for both). Error bars represent 95% confidence interval for the mean. (c) YFP expression as a function of optical density for three genetic backgrounds carrying a P_{srfA}-YFP reporter; ΔQ^{kanR} (light blue), wild-type (light red) and $\Delta Q^{kanR};Q^{+}$ (dark red). (d) YFP as a function of optical density for co-cultures of the wild-type (blue) and ΔQ^{kanR} (red), both encoding for the P_{srfA}-YFP reporter and a distinguishing fluorescent color. (e) Wild-type to ΔQ^{kanR} response ratio as a function of YFP expression of the wild-type (orange). As a control, the YFP ratios for two differentially marked $\Delta Q^{kanR};Q^{+}$ strains are shown (gray, reproduced from Fig. 1c). Expression of the ΔQ^{kanR} strain is higher than that of the wild-type in each co-culture ($p<10^{-20}$ two-sampled t-test, n=32). In (c-e), each data point represents a separate measurement. Series of experiments over varying optical densities were repeated multiple times over at least three days.

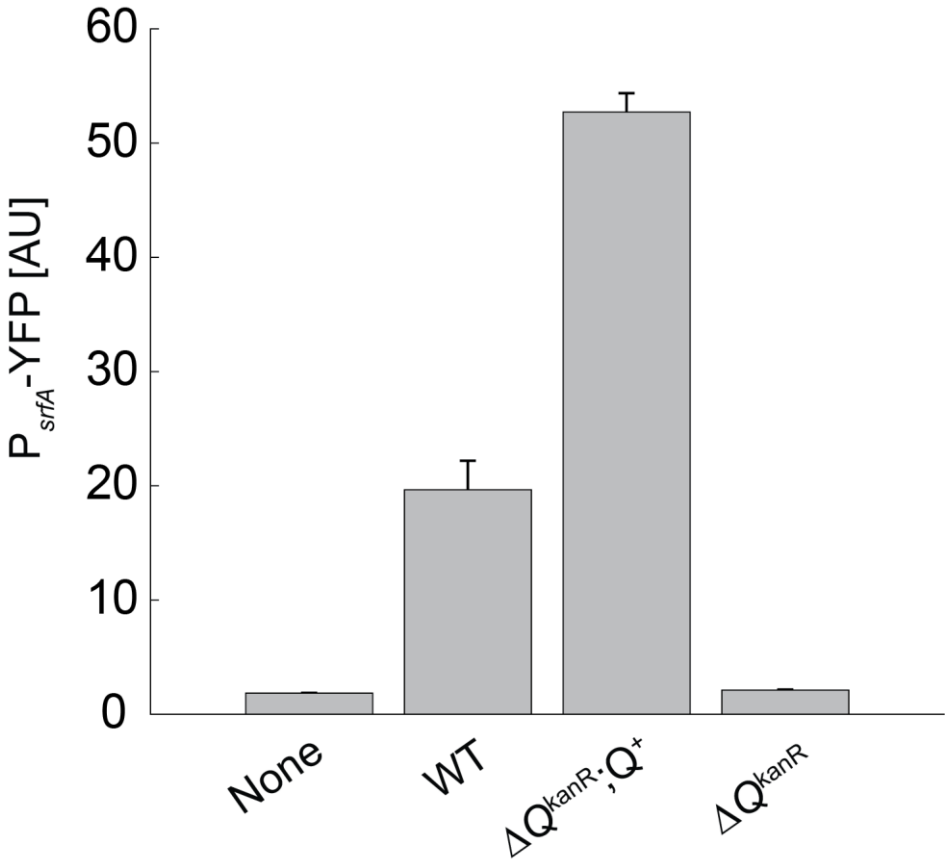

Supplementary Figure 3: The complemented $\Delta Q^{kanR};Q^{+}$ strain produces more autoinducer than the wild-type strain. YFP levels from a P^{ind} strain (induced with 100mM IPTG) to which media conditioned by different strains were added (none: no conditioned medium was added). Conditioned medium was collected from cultures grown to an early stationary state. The genotypes used were wild-type, $\Delta Q^{kanR};Q^{+}$ and ΔQ^{kanR}. Differences between all strains (and specifically the wild-type and $\Delta Q^{kanR};Q^{+}$, as indicated by asterics) were statistically significant ($p<10^{-4}$, two sampled t-test, n=8). Each condition was measured four times. All data points are given in Supplementary File 1.

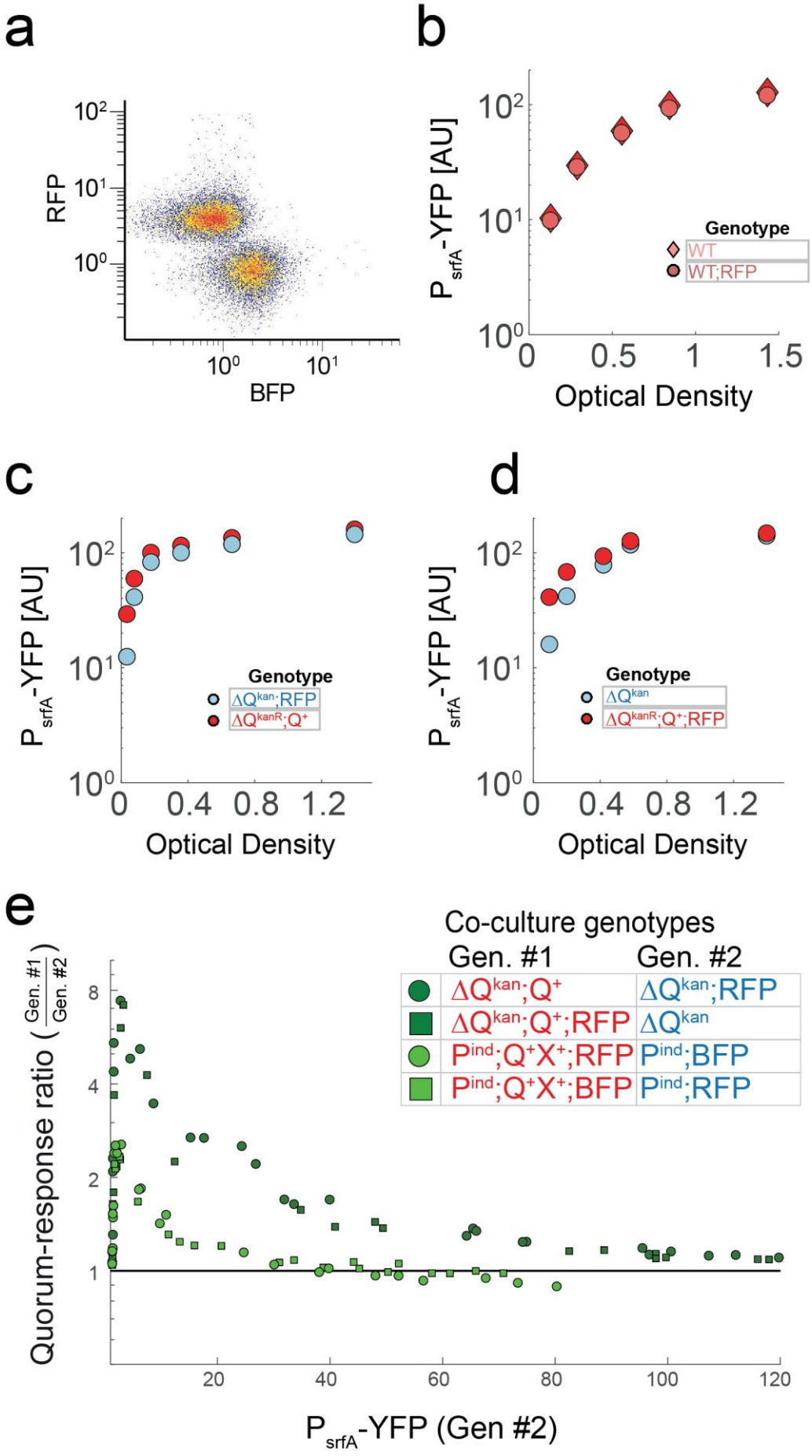
a
RFP
BFP
b
P_{srfA}-YFP [AU]
Optical Density
Genotype
WT
WT;RFP
c
P_{srfA}-YFP [AU]
Optical Density
Genotype
ΔQ^{kan};RFP
ΔQ^{kanR};Q^+
d
P_{srfA}-YFP [AU]
Optical Density
Genotype
ΔQ^{kan}
ΔQ^{kanR};Q^+;RFP
e
Co-culture genotypes
Gen. #1
Gen. #2
ΔQ^{kan};Q^+
ΔQ^{kan};RFP
ΔQ^{kan};Q^+;RFP
ΔQ^{kan}
P^{ind};Q^+X^+;RFP
P^{ind};BFP
P^{ind};Q^+X^+;BFP
P^{ind};RFP
Quorum-response ratio ($\frac{Gen.\ \#1}{Gen.\ \#2}$)
P_{srfA}-YFP (Gen #2)

Supplementary Figure 4: Fluorescent cell identifiers do not affect P_{srfA}-YFP reporter measurements. (a) Example of flow-cytometry results for co-culture of cells expressing constitutive RFP and constitutive BFP. The distinction between the two cell types is clear. (b-d) Shown are fluorescence levels of a P_{srfA}-YFP reporter, as a function of optical density for a co-culture of (b) two strains with $\Delta Q^{kanR};Q^{+}$ genotype, but with one strain also encoding for a constitutively expressed RFP gene. (c,d) two strains with the $\Delta Q^{kanR};Q^{+}$ and ΔQ^{kanR} genotypes, where the RFP-distingushing gene is integrated into the (c) $\Delta Q^{kanR};Q^{+}$ or into the (d) ΔQ^{kanR} strain. In both cases, the autoinducer-producing strain had a higher YFP level than the non-secreting strain. (e) is a reproduction of the response ratio data of Fig. 1c in the main manuscript, for all co-cultures of $\Delta Q^{kanR};Q^{+}$ and ΔQ^{kanR} strains. In Fig. 1c, all points are shown with the same marker, while here the data is separated according to the identity of the RFP-encoding strain: the ΔQ^{kanR} strain (circle) or the $\Delta Q^{kanR};Q^{+}$ strain (square). Each data point represents a separate measurement. Series of experiments over varying optical densities were repeated multiple times over at least three days.

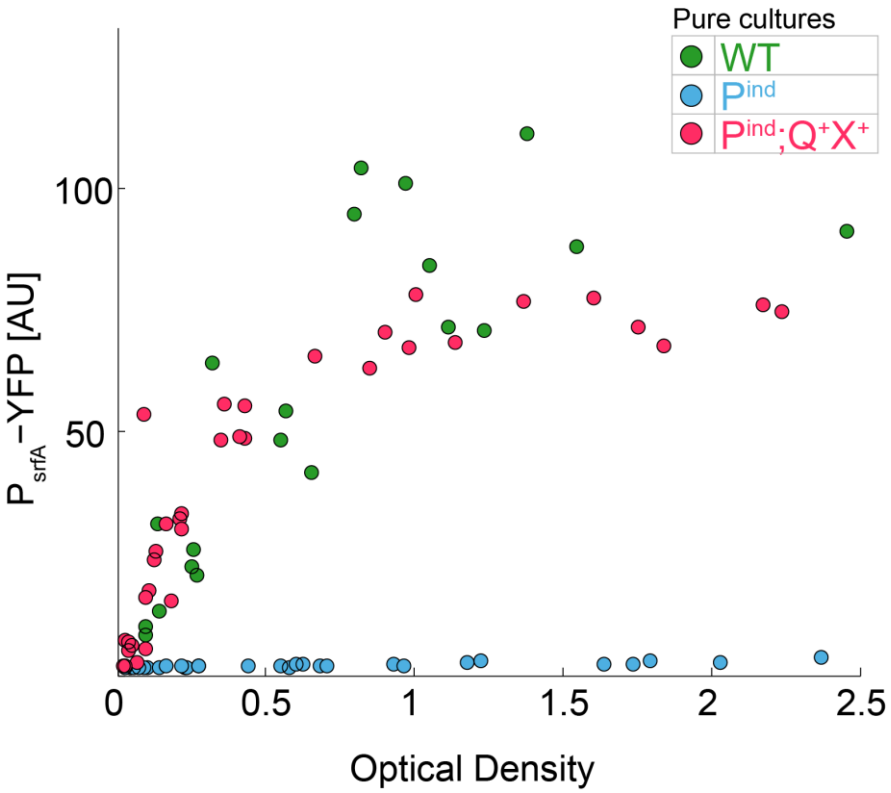

Supplementary Figure 5: The *P*^{ind} response has physiological quorum-sensing dynamics. YFP expression by a P_{srfA}-YFP reporter as a function of optical density for three strains: wild-type (green), the *P*^{ind} strain (cyan), which expresses an inducible *comP* allele and is deleted for the *comQXP* operon and the *P*^{ind}*;Q*$^{+}$*X*$^{+}$ strain (magenta), where the *comQX* genes under their native promoter are integrated into the *P*^{ind} strain. Inducible systems were induced with 100µM IPTG. Each data point represents a separate measurement. Series of experiments over varying optical densities were repeated multiple times over at least three days.

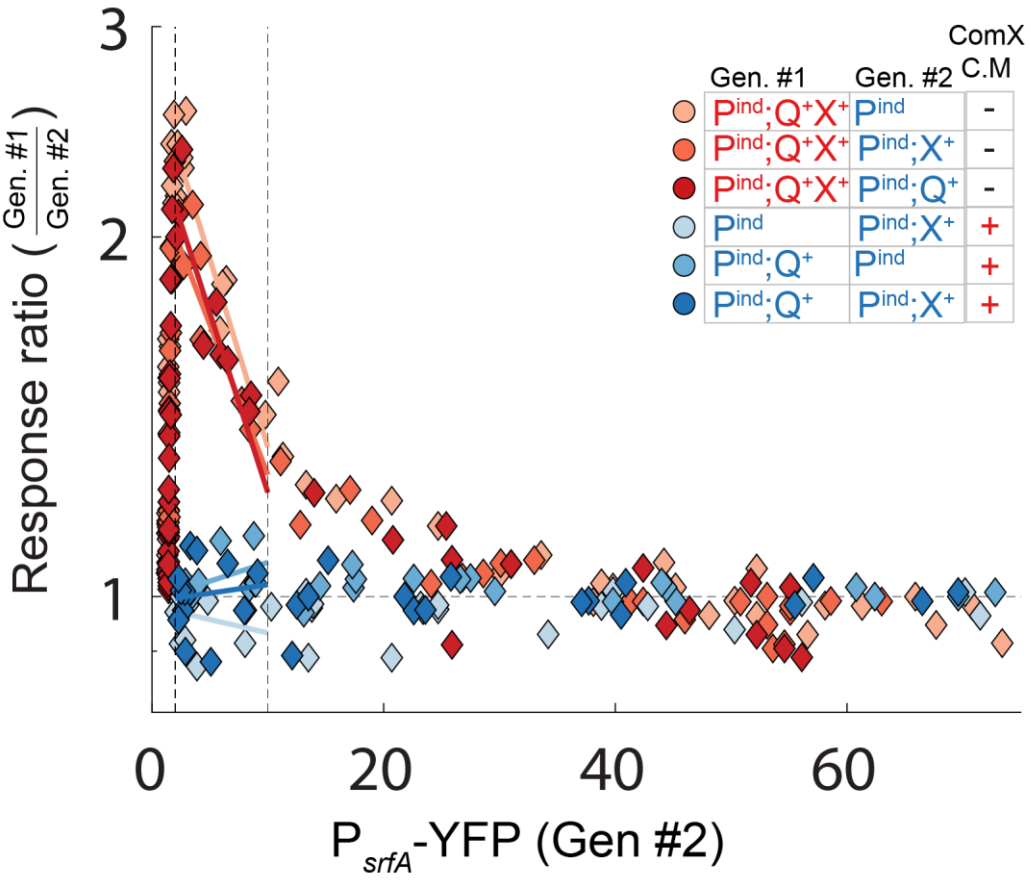

Supplementary Figure 6: Self-sensing depends on the expression of both *comQ* and *comX*. Quorum-sensing response ratio of pairs of co-cultured variants encoding the P^{ind} allele with or without *comX* and *comQ* (see legend for the different pairs). Fig. 1d is based on linear interpolation of the data between the two vertical dashed lines of each co-culture to the expected value indicated by the left dashed line. The linear fit of the data for each pair is also marked. Note that the color code used here are different than those used in Fig. 1d, for clarity.

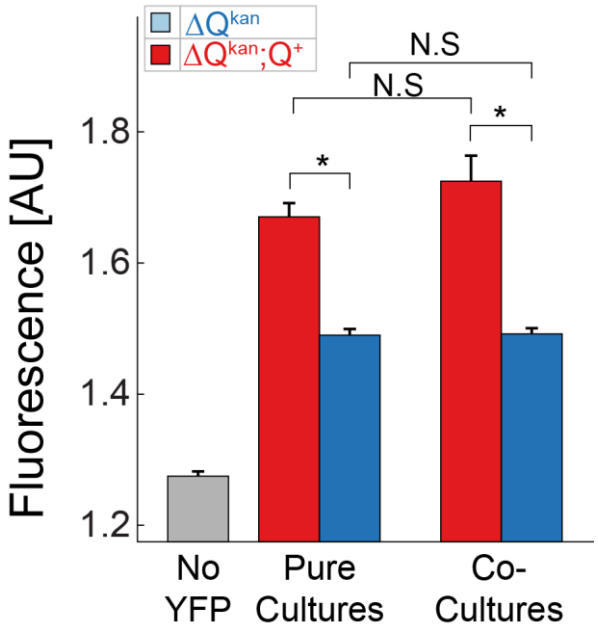

Supplementary Figure 7: ComX-secreting strain has a higher response than non-secreting strain at very low densities. Fluorescence from a ComX secreting (red) and non-secreting (blue) strains at very low densities (methods). Strains were either grown in pure cultures or in co-culture, as indicated. A wild-type strain with no YFP reporter was used to measure autofluorescence (gray). Asterisks and N.S. mark statistically significant and non-significant differences . All measurement with a YFP reporter are significantly higher than background auto-fluorescence. All data points are given in Supplementary File 1.

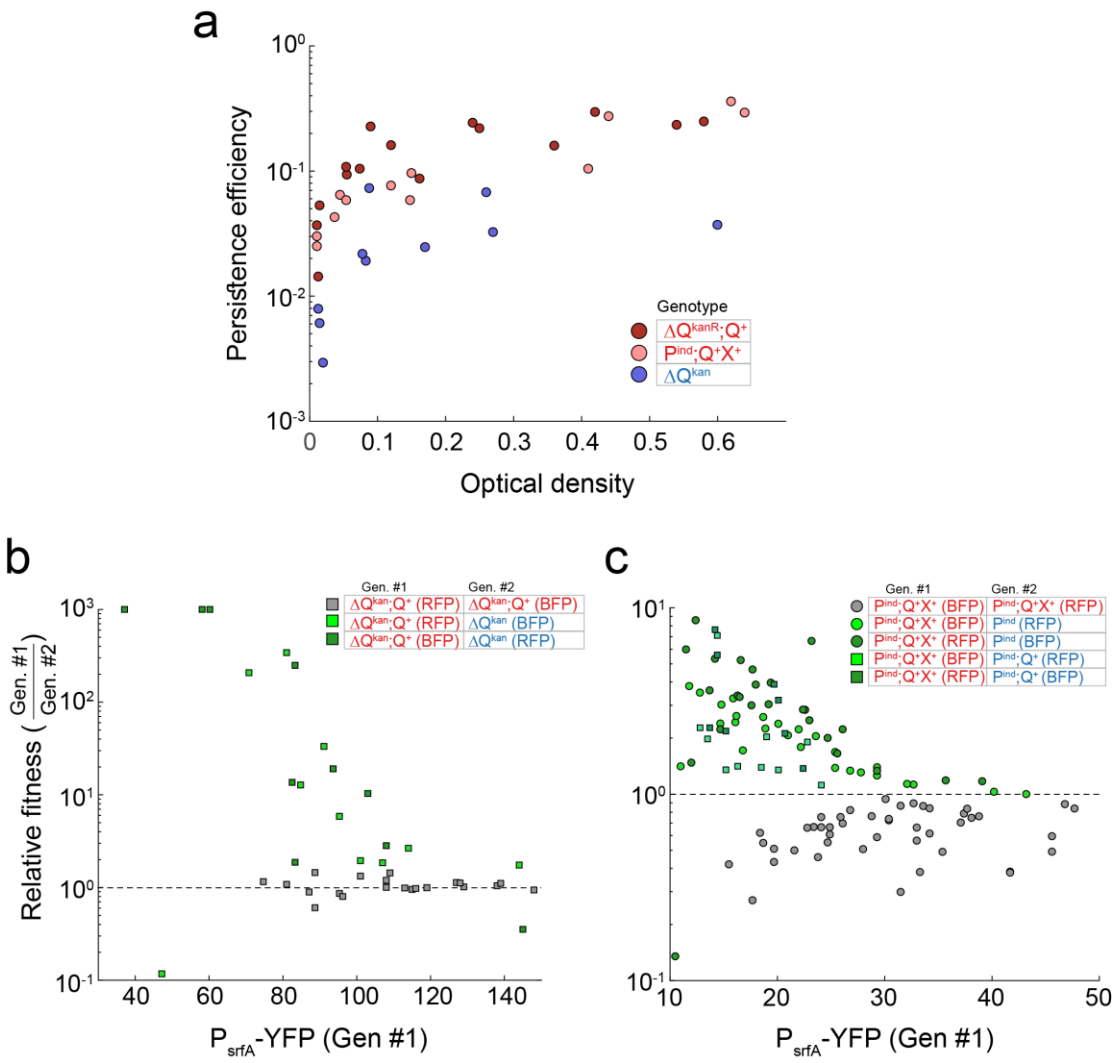

Supplementary Figure 8: Persistence to antibiotics and self-sensing. (a) The persistence levelversus the number of colony forming units prior to antibiotics administration, for three strains: a quorum-sensing mutant (*ΔQ*^{kanR} strain, blue), a strain with approximately physiological levels of quorum-sensing (*P*^{ind}*;QX*$^{+}$, bright red) and a strain with an overexpressed quorum-sensing system (*ΔQ*^{kanR}*;Q*$^{+}$, dark red). (b) Relative fitness of ComX-secreting over non-secreting strains for the strongly activated quorum-sensing system (*ΔQ*^{kanR}*;Q*$^{+}$ vs. *ΔQ*^{kanR}, red). As a control, shown are the results of a producer vs. producer (*ΔQ*^{kanR}*;Q*$^{+}$ vs. *ΔQ*^{kanR}*;Q*$^{+}$, blue). Data were collected and analyzed as explained in Fig. 3 of the main text and Methods. Fitness value of 10^3 implies that the disadventged strain was not observed. (c) Relative fitness of ComX-secreting over non-secreting strains in co-culture under

antibiotic persistence conditions. Show are data for competitions between: physiological ComX-secreting($P^{ind};Q^{+}X^{+}$) and a non-secreting strains, where either RFP (dark green) or BFP (light green, reproduced from Fig. 3) was expressed in the secreting strain. The non-secreting strain either encoded (squares) or did not encode (circles) *comQ.* For clarity, shown are also the results of the control competitions of two secreting strains ($P^{ind};QX^{+}$ vs. $P^{ind};QX^{+}$, gray circles, reporduced from Fig. 3). In the case where *comQ* was expressed in the non-secreting strain, the secreting and non-secreting strains differed only in the expression of *comX*, but had the same integration sites and antibiotic resistance genes insertions (Supplementary Table 1). Note that the secreting strain in Fig. 3 had one more integration site and an extra CmR gene compared to the non-secreting strain (Supplementary Table 1). The essentially identical results of the two competition types indicates that these genomic differences are not important. Each data point represents a separate measurement. Series of experiments over varying optical densities were repeated multiple times over at least three days.

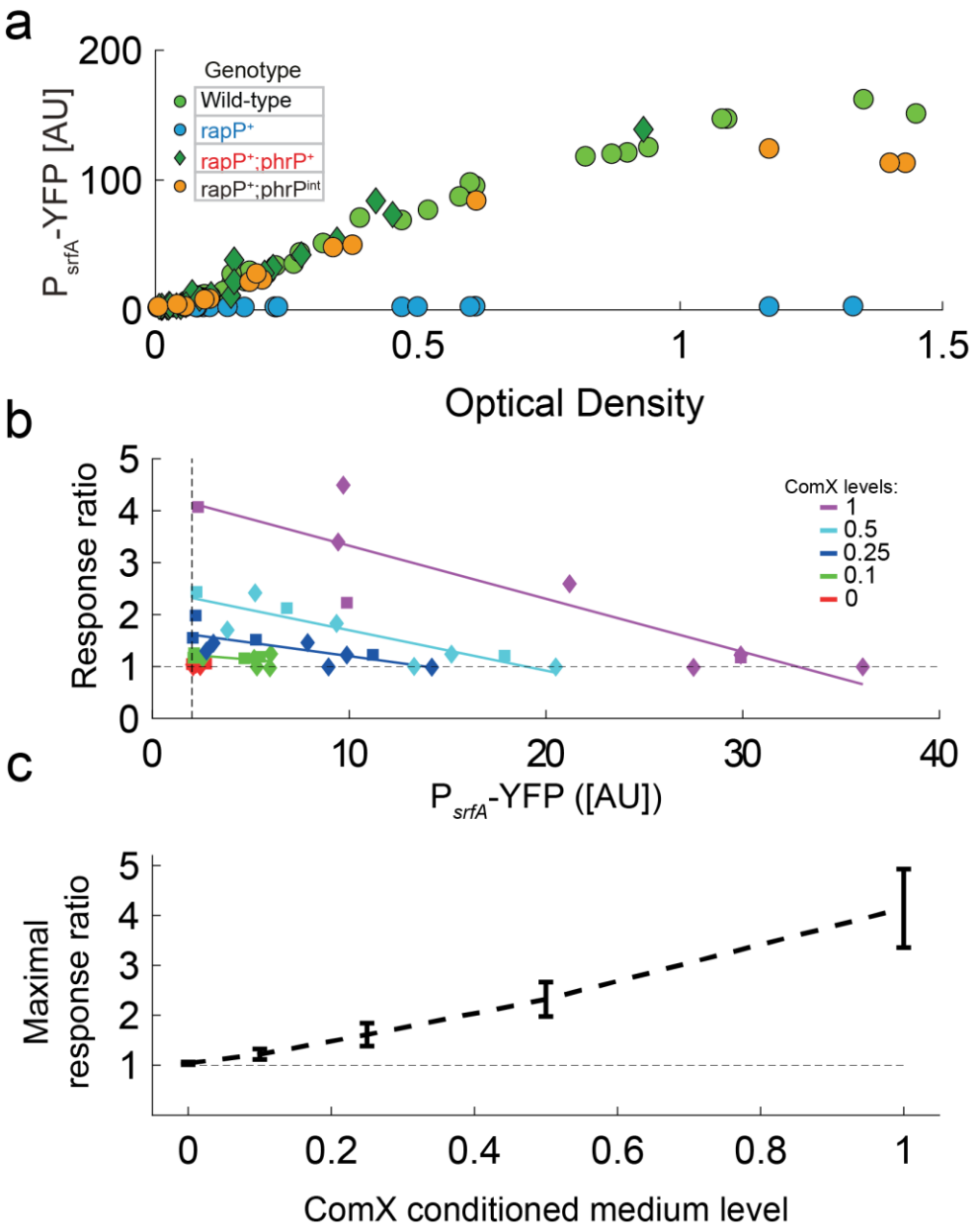

Supplementary Figure 9: RapP-PhrP activity and co-dependence on ComX activity. (a) Expression as a function of cell density in pure cultures of the strains described in the inset legend. (b) A co-culture of *rapP⁺;phrP⁺* and *rapP⁺* strains was grown to a low density and different levels of conditioned medium from a ComX-producing *E. coli* were added. The total level of conditioned medium was kept constant by adding conditioned medium from a background *E. coli* strain. Shown is the response ratio of a P_{srfA}-YFP reporter as function of the YFP expression of the *rapP⁺* strain. Variability arises from measuring quorum-sensing response

at different times after the addition of conditioned medium, different intial density of cells when conditioned medium is added and day to day variability. Different colors mark the level of ComX conditioned medium added (see legend). Lines represent the linear regression best fit of the data for each level. Horizontal dashed line at a value of one. Vertical dashed line at a YFP value of 2. (c) Maximal quorum-sensing response ratio as a function of ComX conditioned medium level. Best estimation for the level of quorum-sensing response at a YFP level of 2 of the *rapP*$^{+}$ strain are based on the linear regression shown in (b). Error bars mark the level of deviation where 50% of observations are expected.

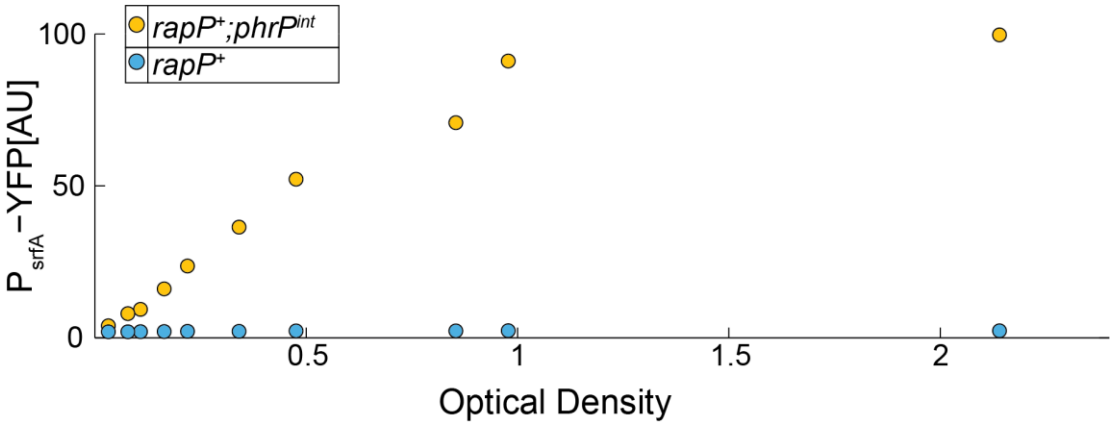

Supplementary Figure 10: The *phrP^{int}* allele acts cell-autonomously. YFP expression of co-cultured *rapP^{+}* (blue) and *rapP^{+};phrP^{int}* (orange). The *phrP^{int}* allele lacks the N-terminal 25 amino-acids of PhrP, comprising the secretion signal sequence. Its coded protein sequence is MSEQSTYKV**ADRAAT**, where the last six amino-acids (highlighted in bold font) constitute the mature peptide. Gene expression has a strictly non-autonomous impact on the P_{srfA}-YFP reporter expression. Each data point represents a separate measurement. Series of experiments over varying optical densities were repeated multiple times over two days.

Supplementary Tables

Supplementary Table 1: strain list

Escherichia coli strains[a]				
Strain name	**Background**	**Genotype**	**Reference**	**Strain designation (used in Figure)[b]**
AEC361	MG1655	*Escherichia coli* K-12 wild type	Lab stock	Used for producing conditioned media in Figures 2C,D,E; S9B,C.
AEC1019	MG1655	ECE174::P_{comQXP}-*comQX* Cm Amp	This study	Used for producing ComX-conditioned media in Figures 2C,D,E; 4A,B; S6; S9B,C.
AEC777	DH5α	pDR111	[1]	
AEC310	DH5α	ECE174	[2]	
AEC839	DH5α	ECE174::P_{comQXP}-*comQ* Cm Amp	This study	
AEC840	DH5α	ECE174::P_{comQXP}-*comQX* Cm Amp	This study	
AEC975	DH12	ECE174::P_{comQXP}-*comX* Cm Amp	This study	
AEC1002	DH12	pDR111::P_{hs}-*comP* Spec Amp	This study	
AEC962	DH12	pDL30::P_{comQXP}-3xYFP Spec Amp	Lab stock	
AEC735	DH12	ECE174::P_{rapP}-$rapP^{T236N}$ Cm Amp	[3]	
AEC1245	DH12	pDL30::P_{comQXP}-$rapP^{T236N}$ Spec Amp	This study	
AEC804	DH12	ECE59::P_{43}-sRBS-mCherry Cm Erm	Lab stock	
AEC806	DH12	ECE59::P_{43}-sRBS-2x mTag-BFP Cm Erm	Lab stock	
AEC1272	DH5α	pDR111::P_{hs}-*phrP* Spec Amp	This study	
AEC1273	DH5α	pDR111::P_{hs}-$phrP^{int}$ Spec Amp	This study	
Bacillus subtilis strains				
Strain name	**Background**	**Genotype**	**Reference**	**Strain designation (used in Figure)**
AES101	PY79	*Bacillus subtilis* PY79 wild type	Bacillus genetic stock center	
AES1334	PY79	*amyE*::(P_{srfA}-3xYFP Spec)	[3]	Wild-type (1C; S2B,C,E; S4A)
AES1367	PY79	*zba88*::(*amyE'*::P_{srfA}-3xYFP Spec Cm Kan)	[3]	Wild-type (S5)
BD2876	168	his leu met *srfA*-lacZ tet, Δ*comQ*::Kan	[4]	
AES1980	PY79	*amyE*::(P_{srfA}-3xYFP Spec), Δ*comQ*::Kan	BD2876→AES1334	ΔQ^{kanR} (1B,C; S2A,B,C,D,E; S4C,D)
AES2665	PY79	*lacA*::(P_{43}-YFP mls), *ppsB*::(P_{trpE}-*mCherry* Ph)	Lab stock	
AES2107	PY79	*amyE*::(P_{srfA}-3xYFP Spec), Δ*comQ*::Kan, *ppsB*::(P_{trpE}-*mCherry* Ph)	AES2665→AES1980	ΔQ^{kanR} (red alternative) (1C; S2C,E; S4B,D)

AES2048	PY79	*amyE*::(P_{srfA}-3xYFP Spec), Δ*comQ*::Kan, *sacA::(*P_{comQXP}-*comQ* Cm)	AEC839→AES1980	*ΔQ^{kanR};Q^{+}* (1C; S2B,C; S4B,D)
AES2172	PY79	*amyE*::(P_{srfA}-3xYFP Spec), Δ*comQ*::Kan, *sacA::(*P_{comQXP}-*comQ* Cm), *ppsB*::(P_{trpE}-*mCherry* Ph)	AES2665→AES2048	*ΔQ^{kanR};Q^{+}* (red alternative) (1B,C; S2C; S4C,D)
AES2124	PY79	*amyE*::(P_{srfA}-3xYFP Spec), *ppsB*::(P_{trpE}-*mCherry* Ph)	AES2665→AES1334	Wild-type (red alternative) (1C; S2C,D,E; S4A)
AES2111	PY79	Δ*comQXP*::Tet	[5]	
AES2961	PY79	*amyE*::(P_{hs}-*comP* Spec)	AEC1002→AES101	
AES2962	PY79	*amyE*::(P_{hs}-*comP* Spec), *sacA*::(P_{comQXP}-*comX* Cm)	AEC975→AES2961	
AES2977	PY79	*amyE*::(P_{hs}-*comP* Spec), *sacA*::(P_{comQXP}-*comQX* Cm)	AEC840→AES2961	
AES2978	PY79	*amyE*::(P_{hs}-*comP* Spec), *sacA*::(P_{comQXP}-*comQ* Cm)	AEC839→AES2961	
AES3215	PY79	ECE59::P_{43}-sRBS-mCherry Cm Erm	AEC804→AES101	No YFP (4B; S7)
AES3216	PY79	ECE59::P_{43}-sRBS-2x mTag-BFP Cm Erm	AEC806→AES101	No YFP (4B; S7)
AES3132	PY79	*amyE*::(P_{hs}-*comP* Spec), *zba88*::(*amyE'*::P_{srfA}-3xYFP Spec Cm Kan), ECE59::P_{43}-sRBS-mCherry Cm Erm; Δ*comQXP*::Tet	AES2111→AES3124	*P^{ind}* (red alternative, plasmid) (1C,D; 2E; 3; S3; S4D; S5; S6; S8C)
AES3133	PY79	*amyE*::(P_{hs}-*comP* Spec), *zba88*::(*amyE'*::P_{srfA}-3xYFP Spec Cm Kan), ECE59::P_{43}-sRBS-2x mTag-BFP Cm Erm, Δ*comQXP*::Tet	AES2111→AES3125	*P^{ind}* (blue alternative, plasmid) (1C,D; 2D,E; S3; S4D; S5; S6; S8C)
AES3134	PY79	*amyE*::(P_{hs}-*comP* Spec), *sacA::(*P_{comQXP}-*comX* Cm), *zba88*::(*amyE'*::P_{srfA}-3xYFP Spec Cm Kan), ECE59::P_{43}-sRBS-mCherry Cm Erm, Δ*comQXP*::Tet	AES2111→AES3126	*P^{ind};X^{+}* (red alternative, plasmid) (1D; S6)
AES3135	PY79	*amyE*::(P_{hs}-*comP* Spec), *sacA::(*P_{comQXP}-*comX* Cm), *zba88*::(*amyE'*::P_{srfA}-3xYFP Spec Cm Kan), ECE59::P_{43}-sRBS-2x mTag-BFP Cm Erm, Δ*comQXP*::Tet	AES2111→AES3127	*P^{ind};X^{+}* (blue alternative, plasmid) (1D; S6)
AES3136	PY79	*amyE*::(P_{hs}-*comP* Spec), *sacA::(*P_{comQXP}-*comQX* Cm), *zba88*::(*amyE'*::P_{srfA}-3xYFP Spec Cm Kan), ECE59::P_{43}-sRBS-mCherry Cm Erm, Δ*comQXP*::Tet	AES2111→AES3128	*P^{ind};Q^{+}X^{+}* (red alternative, plasmid) (1C,D; 3; S4D; S5; S6; S8A,C)
AES3137	PY79	*amyE*::(P_{hs}-*comP* Spec), *sacA::(*P_{comQXP}-*comQX* Cm), *zba88*::(*amyE'*::P_{srfA}-3xYFP Spec Cm Kan), ECE59::P_{43}-sRBS-2x	AES2111→AES3129	*P^{ind};Q^{+}X^{+}* (blue alternative, plasmid) (1C,D; 3; S4D; S5; S6; S8A,C)

		mTag-BFP Cm Erm, Δ*comQXP*::Tet		
AES3138	PY79	*amyE*::(P_{hs}-*comP* Spec), *sacA::(*P_{comQXP}-*comQ* Cm), *zba88*::(*amyE'*::P_{srfA}-3xYFP Spec Cm Kan), ECE59::P_{43}-sRBS-mCherry Cm Erm, Δ*comQXP*::Tet	AES2111→AES3130	P^{ind};Q^{+} (red alternative, plasmid) (1D; S6; S8C)
AES3139	PY79	*amyE*::(P_{hs}-*comP* Spec), *sacA::(*P_{comQXP}-*comQ* Cm), *zba88*::(*amyE'*::P_{srfA}-3xYFP Spec Cm Kan), ECE59::P_{43}-sRBS-2x mTag-BFP Cm Erm, Δ*comQXP*::Tet	AES2111→AES3131	P^{ind};Q^{+} (blue alternative, plasmid) (1D; S6; S8C)
AES3563	PY79	*amyE*::(P_{srfA}-3xYFP Spec), ECE59::P_{43}-sRBS-mCherry Cm Erm	AEC804→AES1334	Wild-type (red alternative, plasmid) (S3)
AES3564	PY79	*amyE*::(P_{srfA}-3xYFP Spec), ECE59::P_{43}-sRBS-2x mTag-BFP Cm Erm	AEC806→AES1334	Wild-type (blue alternative, plasmid) (S3)
AES3565	PY79	*amyE*::(P_{srfA}-3xYFP Spec), Δ*comQ*::Kan, *sacA::(*P_{comQXP}-*comQ* Cm), ECE59::P_{43}-sRBS-mCherry Cm Erm	AEC804→AES2048	ΔQ^{kanR};Q^{+} (red alternative, plasmid) (2C,E; S3; S7; S8A,B)
AES3566	PY79	*amyE*::(P_{srfA}-3xYFP Spec), Δ*comQ*::Kan, *sacA::(*P_{comQXP}-*comQ* Cm), ECE59::P_{43}-sRBS-2x mTag-BFP Cm Erm	AEC806→AES2048	ΔQ^{kanR};Q^{+} (blue alternative, plasmid) (2E; S3; S7; S8A,B)
AES3567	PY79	*amyE*::(P_{srfA}-3xYFP Spec), Δ*comQ*::Kan, ECE59::P_{43}-sRBS-mCherry Cm Erm	AES1980→AES3563	ΔQ^{kanR} (red alternative, plasmid) (2D,E; S3; S7; S8A,B)
AES3568	PY79	*amyE*::(P_{srfA}-3xYFP Spec), Δ*comQ*::Kan, ECE59::P_{43}-sRBS-2x mTag-BFP Cm Erm	AES1980→AES3564	ΔQ^{kanR} (blue alternative, plasmid) (2C,E; S3; S7; S8A,B)
AES1477	PY79	*amyE*::(P_{srfA}-3xYFP Spec), *amyE'::*(P_{hs}-*phrP* Spec Cm Kan)	[3]	
AES2539	PY79	*sacA::*(P_{srfA}-3xYFP Cm)	[6]	
AES4136	PY79	*sacA::*(P_{srfA}-3xYFP Cm), ECE59::P_{43}-sRBS-2x mTag-BFP Cm Erm	AEC806→AES2539	Wild-type (blue alternative, plasmid) (S9A)
AES4137	PY79	*sacA::*(P_{srfA}-3xYFP Cm), ECE59::P_{43}-sRBS-mCherry Cm Erm	AEC804→AES2539	Wild-type (red-alternative, plasmid) (S9A)
AES4141	PY79	*sacA::*(P_{srfA}-3xYFP Cm), ECE59::P_{43}-sRBS-mCherry Cm Erm, *amyE*::(P_{comQXP}-$rapP^{T236N}$ Spec)	AEC1245→AES4137	*rapP*$^{+}$ (red alternative, plasmid) (4A,B; S9A,B,C; S10)
AES4208	PY79	*sacA::*(P_{srfA}-3xYFP Cm), ECE59::P_{43}-sRBS-2x mTag-BFP Cm Erm, *amyE*::(P_{comQXP}-$rapP^{T236N}$ Spec)	AEC1245→AES4136	*rapP*$^{+}$ (blue alternative, plasmid) (4A,B; S9A,B,C)
AES4158	PY79	*sacA::*(P_{srfA}-3xYFP Cm), ECE59::P_{43}-sRBS-mCherry Cm Erm *amyE*::(P_{comQXP}-$rapP^{T236N}$	AES1477→AES4141	*rapP*$^{+}$;*phrP*$^{+}$ (red alternative, plasmid) (4A,B; S9A,B,C)

		Spec), *amyE'*::(P_{hs}-*phrP* Spec Cm Kan)		
AES4214	PY79	*sacA*::(P_{srfA}-3xYFP Cm), ECE59::P_{43}-sRBS-2x mTag-BFP Cm Erm *amyE*::(P_{comQXP}-*rapP*^{T236N} Spec), *amyE'*::(P_{hs}-*phrP* Spec Cm Kan)	AES1477→AES4208	*rapP*$^{+}$;*phrP*$^{+}$ (blue alternative, plasmid) (4A,B; S9A,B,C)
AES4344	PY79	*amyE'*::(P_{hs}-*phrP*^{int} Spec Cm Kan)	AEC1273→AES827	
AES4425	PY79	*sacA*::(P_{srfA}-3xYFP Cm), ECE59::P_{43}-sRBS-2x mTag-BFP Cm Erm *amyE*::(P_{comQXP}-*rapP*^{T236N} Spec), *amyE'*::(P_{hs}-*phrP*^{int} Spec Cm Kan)	AES4344→AES4208	*rapP*$^{+}$;*phrP*^{int} (S9A; S10)

[a] DH12 and DH5α *E.coli* strains were used for cloning and MG1655 strain for condition medium due to its ability to grow in minimal media.

[b] Numbers followed by letter (e.g., 4A) designate the relevant main manuscript figure. A capital S prior to the number (e.g., S8D) designate a supplementary figure.

Supplementary Table 2: primers list

Name	Sequence	Enzyme
comP-RT-F	TCGAAGAAAAACAGCGTTCA	
comP-RT-R	AGCTTGTCCTGCACCTCTTC	
rpoB-RT-F	TCGTTACCTTGGCATTCACA	
rpoB-RT-R	CACGGTTATCAAACGGCTCT	
bglA-RT-F	GACGGCGATGATGAGATTTT	
bglA-RT-R	TGTACGGATTTTCGACACCA	
ComP-NheI-R	TATAGCTAGCCCATTACAATTCGATTTCAATATCAGCC	NheI
ComP-nativeRBS-F	CTAAGTCGACGATTATTATCTGGCTGATCC	SalI
ComQ-into-ECE174-F-[BamHI]	ATGCGGATCCAATTTCGTGAAAAAGACTTGGAAACA	BamHI
ComQ-into-ECE174-R-[EcoRI]	ATGCGAATTCTTAGGTCTTGCATCTTGTATCCCC	EcoRI
ComQX-into-ECE174-R-[EcoRI]	ATGCGAATTCTTAATCACCCCATTGACGGGT	EcoRI
dcomQ-R	GGAAATATATAAACAGAAATGTATTTCTGC	
dcomQ-F	CCTTCATTTTCTCCTTGATCCGG	
RapP-SphI-R	ATGAAGCATGCTTACATTTTTTCATTTAAATG	SphI
hsRapP-F	ATCCAGCTAGCAAAGAAAAGGAGGTATTTGATTG	NheI
PQXP-NheI-R	CTTAGCTAGCCTCCTTGATCCGGACAGAATC	NheI
pDL30-SphI-F	ATTGCGCATGCCATATGATACCGTCGGGCGG	SphI
PhrP-SalI-F	ATTGGTCGACCAAAGGGGGAAACATTTAAATGAAAAAATG	SalI
PhrP-NheI-R	ATTGGCTAGCCCTTTATCATATTAAGTTGC	NheI
PhrP-NO-signal-seq-R	CATTTAAATGTTTCCCCCTTTG	
PhrP-NO-signal-seq-F	TCTGAGCAGTCCACTTATAAGG	

Supplementary Discussion

Introduction

This supplementary text has four sections in which we use mathematical analysis to study various aspects of self-sensing. In the first section, we use a minimalistic diffusion model to consider the fundamental limit on the ability of cells to perform quorum sensing. In the second section, we consider various processes that can increase self-sensing beyond the fundamental limit. In the third section we consider the expected shape of the response ratio curve, and their relation to the curves we characterize in Figs. 1,4 of the main manuscript. Finally, in the fourth section, we consider the expected change in response curve to external signal for the various models, as discussed and analyzed in Fig. 3 of the manuscript.

Fundamental limit on quorum sensing

To assess the minimal level of self-sensing, we assume that cells are growing exponentially with a doubling time $\boldsymbol{\tau}$ in a well-mixed environment of volume $\boldsymbol{V}$, while secreting an autoinducer molecule at a constant rate, $\boldsymbol{F}\,\frac{\boldsymbol{molecules}}{\boldsymbol{seconds\times cell}}$. The autoinducer accumulates in the environment with no degradation. At the microscopic level, we assume that cells are spherical of radius $\boldsymbol{a}$ and evenly secrete the autoinducer from their surface. The autoinducer does not interact specifically with the cell's outer layer (membrane, cell wall etc.) and its diffusion coefficient is $\boldsymbol{D}$. Finally, we assume that the Kolmogorov mixing length-scale is much larger than the radius of the cell, but much smaller than the dimension of the vessel, which allows us to assume homogenous mean concentration on the one hand and unperturbed local gradients near the cell surface, on the other. The assumption on the Kolmogorov length scales holds for any reasonable level of mixing in our experiment. We will later discuss the impact of failure of other assumptions.

Mean concentration. Using the above assumptions, we find that the average concentration of autoinducer in the well-mixed environment, $\boldsymbol{c_{av}}$, is equal to,

1) $c_{av} = \frac{2FN\tau}{V} = 2F\tau n,$

where $\boldsymbol{n} = \frac{N}{V}$ is the density of cells. As mentioned above, $\boldsymbol{\tau}$ is the doubling time of the bacteria. We note that if the autoinducer is degraded with a time-scale faster than the doubling time, then τ would be the degradation time-scale and not the doubling time (see below).

Local gradient. Using the diffusion equation [7], one can easily find that the concentration of autoinducer near the cell, $\boldsymbol{c(r)}$, as a function of the distance from the cell surface is:

2) $c(r) = (c_a - c_{av})\frac{a}{r} + c_{av}$

, where $\boldsymbol{a}$ is the radius of the cell (assumed spherical for simplicity), r is the distance from the cell's center $(r \geq a)$ and $\boldsymbol{c_a}$ is the concentration on the cell's surface. The relation between flux and concentration can be found from Fick's law:

3) $F = -4\pi a^2 D \frac{dc}{dr}\Big|_{r=a} = 4\pi a D(c_a - c_{av})$

We find therefore that the self-sensing component of the concentration, which is the difference between the concentration on the cell's surface and the average concentration, is:

4) $c_{self} = (c_a - c_{av}) = \frac{F}{4\pi a D}$

The self-sensing component becomes dominant over the average concentration once:

5) $c_{self} = \frac{F}{4\pi a D} > F\tau n = c_{av}$

This implies:

6) $n < \boldsymbol{n_{self}} \equiv \frac{1}{4\pi a D \tau}$

Self-sensing therefore limits the minimal density that can be sensed by the cells. Note that this limit does not depend on the rate of signal production, as this rate determines both the local gradient and the average concentration. The limit is inversely proportional to the autoinducer diffusion rate, to the radius of the cell and to doubling time, which is the typical accumulation time of the signal in the environment.

To get an estimate of this limit, we can use typical values for the above parameters in our experiments, $D_{AI} \sim 10^{-5}\frac{cm^2}{sec}$, $a \sim 10^{-4} cm$ and $\tau \sim 3{,}300\, sec$ as a typical doubling time. The critical self-sensing threshold than turns out to be:

7) $n_{self} \sim 2 \times 10^4 \frac{cells}{ml}$

This is equivalent to an optical density of ~0.0001 – much lower than the actual densities where quorum-sensing response is typically observed. Therefore, the minimalistic self-sensing level does not set a realistic limit on quorum sensing.

We also note that there could be mechanisms that would reduce the level of self-sensing even further. For example, cells could, in principle, secrete and sense at different times, thereby

preventing self-sensing. Alternatively, the signaling molecule could be activated extracellularly with an intrinsic time-delay. For example, extracellular cleavage such as in the Rap-Phr system can reduce the level of self-sensing.

Models for increased self-sensing

The minimalistic effect is not in accordance with what we observe in our experiments, where self-sensing has observable effects at densities with optical densities ~0.01-0.1, corresponding to cell densities of 10^6-10^7 cells/ml. What are the possible explanations for the extremely high level of self-sensing we observe? We provide here four alternative mechanisms and discuss their relevance to the results presented in the main text.

1. **Autoinducer degradation**. If the autoinducer is unstable and spontaneously degrade in the environment in a rate that is faster than the doubling time, than the concentration of autoinducer will depend on the degradation time-scale τ_d instead of the doubling time. For this to compensate for the missing two orders of magnitude of density, the **degradation time has to be of order of 30 seconds.** Degradation varies considerably between different systems and may even depend on the density of cells (if degradation is mediated by internalization of the autoinducer [8]). Nevertheless, degradation rates as high as 30 seconds were never reported, to the best of our knowledge.

2. **Intracellular interactions**. In some quorum-sensing systems, the receptor and autoinducer molecules can interact within the cell. This may lead to direct interaction of the cell-autonomously produced autoinducer with its receptor, prior to its secretion. For example, cytoplasmic interactions can occur during the production of homo-serine-lactone autoinducers, which are used by many Gram negative bacteria. In the synthetic yeast system described in ref [9], alpha factor and alpha receptor may interact within a secretion vessel. In contrast, in the ComQXP QS system, intracellular interactions are less likely, as the ComP receptor is extracellular and is most likely inactive before it is properly inserted into the membrane, with reception domain facing out [10]. The Rap-Phr systems interact within the cell, but Phr maturation requires first that the molecule will be secreted. A leading possibility for self-sensing in the Rap-Phr system is if the Phr molecule has some level of intracellular cleavage.

3. **Receptor-secretion molecular co-localization.** If the receptor is located just adjacent to the secretion complex, at a molecular distance $d \ll a$, and if there are in total N_r secretion-reception complexes, then the self-sensing concentration will be:

8) $\frac{1}{4\pi N_r dD}$

However, efficient reception requires that $N_r d \sim a$ [7], so it is not clear whether this arrangement would significantly change the level of self-sensing, unless efficiency of reception is compromised. We see no clear biological function in either attaching the reception and secretion components to the same complex, or in relaxing the efficiency of sensing. We therefore do not find this hypothesis plausible.

4. **Hydrophobic interaction with cell membrane** as a mechanism for self-sensing

Another mechanism for self-sensing, which we view favorably for the ComQXP system, is that upon secretion, the autoinducer molecule is initially attached to the membrane due to its hydrophobicity. If the membrane-attached autoinducer can activate the receptor, then we expect that the concentration of autoinducer on a secreting cell membrane will be the sum of a self-produced component and of trans-produced autoinducers.

We use the following model to estimate this effect. We denote the attachment and detachment coefficients of the autoinducer to the membrane as k_{mem}, k_{sol}. The equations for the concentration of the membrane-bound ($\boldsymbol{c_{mem}}$) and soluble ($\boldsymbol{c_{sol}}$) autoinducer molecules are:

9) $\frac{dc_{mem}}{dt} = \frac{F}{4\pi a^2} + k_{mem} c_{sol}(a) - k_{sol} c_{mem}$

10) $\frac{\partial c_{sol}}{\partial t} = D\nabla^2 c_{sol};\ D\nabla c_{sol}|_{r=a} = F$

Where F is the production rate of the autoinducer, $c_{sol}(a)$ is the concentration of the soluble autoinducer near the cell surface and c_{mem} is the membrane concentration and a, D are the cell radius and autoinducer diffusion rate.

The solution in steady state of the two equations is therefore:

11) $c_{sol}(a) = \frac{F}{4\pi a D} + c_{av};\ c_{mem} = \frac{k_{mem}}{k_{sol}}\left(\frac{F}{4\pi a D} + c_{av}\right) + \frac{F}{4\pi a^2 k_{sol}}$

In a non-producing cell, we find that the membrane bound concentration by setting $F = 0$ to be:

12) $c_{sol}^{non}(a) = c_{av};\ c_{mem} = \frac{k_{mem}}{k_{sol}} c_{av}$

The self-sensing component is here composed of two component:

13) $c_{self} = c_{mem} - c_{mem}(F = 0) = \left(\frac{k_{mem}}{k_{sol}} \frac{1}{4\pi a D} + \frac{1}{4\pi a^2 k_{sol}}\right) F$

The first term is the diffusion self-gradient component multiplied by the partition coefficient, $\frac{k_{mem}}{k_{sol}}$, and the second term is the membrane influx to outflux balance component.

Setting $c_{av} = 2F\tau n$ as in eq. 1 above, we now find that self-sensing is equal to the quorum-sensing component at:

14) $$n_{self} = \frac{1}{4\pi aD\tau} + \frac{1}{4\pi a^2 k_{mem}\tau} \equiv n_{self,diff} + n_{self,mem}$$

The first component is the diffusion related self-sensing density as in eq. 6 above. The second term is the hydrophobic specific term. Its effect on the threshold depends on its relative ratio to the diffusion term:

15) $$\frac{n_{self,mem}}{n_{self,diff}} = \frac{D/a}{k_{mem}}$$

Impact of self-sensing on response at different densities

In Figs. 1d,4a we show the response ratio curves of the ComQXP and Rap-Phr systems correspondingly. These are characterized by a fairly low ratio at very low densities, which is increased as density increases, reach a maximum, after which the decline with density.

To understand this characteristic shape, we assume that the response function (e.g., activation of a specific promoter) as a function of total sensed autoinducer concentration is an increasing function $F(s) = f_0 + f(s)$, where f_0 is the leakiness of the promoter in the absence of signal and $f(0) = 0$. In addition, measurements are affected by a background threshold f_{th} due to cellular autofluorescence. If we assume that an autoinducer-producing cell has a concentration s_0, then as a function of external signal levels, s, we expect the measured response ratio to behave as:

16) $$R = \frac{f_{th}+f_0+f(s+s_0)}{f_{th}+f_0+f(s)}$$

For the sake of the analysis below, we will combine $f_{th} + f_0$ into the term f_{th}, as both of them contribute to the baseline observed activity in the absence of signal. There are several important limits we can derive from this expression:

I. **Low autofluorescence**: For response levels significantly above detection limit we can approximate, $f_{th} \approx 0$, then $R \approx \frac{f(s+s_0)}{f(s)} \approx s_0 \frac{dlog\, f}{ds}$ will be a decreasing function for any response function which grows more slowly than an exponent. This decrease is what we observe at high cell densities.

II. **High autofluorescence**: In contrast, if f_{th} is large compared to the responses (as may occur at low signal level) than R will be close to 1. Specifically, at $s = 0$, we find: $R = \frac{f_{th}+f(s_0)}{f_{th}} = 1 + \frac{f(s_0)}{f_{th}} \approx 1 + \frac{1}{f_{th}} \frac{df}{ds}\Big|_{s=0} s_0$. The difference from 1 will therefore depend on the size of the self-sensing signal AND on the steepness of the response function near $s = 0$. Various mechanisms can lead to a steep gradient at low concentrations. For example, if unbound receptor acts as a phosphatase of the response regulator response at low concentration may become steeper.

III. **High self-sensing signal**: If the self-sensing concentration, s_0, is significant for passing the threshold between the two states, $f(s) < f_{th} < f(s + s_0)$, then $R \approx 1 + \frac{f(s+s_0)}{f_{th}}$ is an increasing function of s. This may explain the rise we see at low densities with the two systems.

Altogether, this analysis implies that if the self-sensing autoinducer concentration is insufficient to strongly induce the cells, but the response is sufficiently non-linear, than we expect to find the observed response ratio curve approaching a ratio of one at very low concentrations, follow by a fast increase and a slower decrease.

We note that once we correct for autofluorescence levels, the response curve in the ComQXP system reaches a ratio of two at very low densities (Supplementary Figure 7). The fact that it is still increasing (up to a factor of ~8) is probably due to the leakiness of the system in the absence of signal as can be seen from the response levels of the ΔQ^{kanR} mutant at low densities. When we correct for autofluorescence in the Rap-Phr system, we get a response ratio which is larger than 10 at low densities. This would probably just decrease with a function of density, however, the additional autofluorescence induced by the conditioned medium make the analysis more complicated.

Expected response curves for the over-reception and self-sensing model

In the work, we argued that we would expect to find parallel left-shift of the response curves for a slef-sensing model and a change in slope of the response curve for an over-reception model. Here we briefly explain the underlying assumptions for these two expectations.

a. **Self-sensing model**: The expected left shift is intrinsically assumed in the above section when we state that the impact of self-sensing is simply to shift the perceived concentration from s to $s + s_0$. Essentially, this requires us to assume that the concentration of self-sensed autoinducer is independent of external signal. This will not be true if there is a positive feedback on autoinducer production. At least in the case of

the ComQXP system, this is known to be the case as a ComA mutant produces autoinducer at a comparable level to that of the wild-type [11]. An effective feedback can occur if, for example, external signal interferes with the diffusion or transport of self-secreted signal. Again, there is no data on such behavior for the systems we have studied and as export is typically energy-dependent, we do not expect it to strongly depend on the external concentration.

b. Over-reception: Here, our main assumption is that, at least at low concentration of the autoinducer, bound-receptor serves as the active limit on signaling. Assuming a simple binding kinetic model, $R + AI \leftrightharpoons R \cdot AI$, one would find that:

$$[R \cdot AI] = \frac{s}{K + s} R^{tot} \cong \frac{s}{K} R^{tot},$$

Where s is the level of autoinducer and R^{tot} is the total level of receptor. The level of active complex is therefore directly proportional to the total level of receptor. Over-reception should therefore lead to changes in the relation between active receptor levels and external autoinducer levels and these would be reflected in the response function.

References

1. Doan, T., K.A. Marquis, and D.Z. Rudner, *Subcellular localization of a sporulation membrane protein is achieved through a network of interactions along and across the septum.* Molecular Microbiology, 2005. **55**(6): p. 1767-1781.
2. Middleton, R. and A. Hofmeister, *New shuttle vectors for ectopic insertion of genes into Bacillus subtilis.* Plasmid, 2004. **51**(3): p. 238-245.
3. Bendori, S.O., et al., *The RapP-PhrP Quorum-Sensing System of Bacillus subtilis Strain NCIB3610 Affects Biofilm Formation through Multiple Targets, Due to an Atypical Signal-Insensitive Allele of RapP.* Journal of bacteriology, 2015. **197**(3): p. 592-602.
4. Tortosa, P., et al., *Specificity and Genetic Polymorphism of the Bacillus Competence Quorum-Sensing System.* J. Bacteriol., 2001. **183**(2): p. 451-460.
5. Pollak, S., et al., *Facultative cheating supports the co-existence of multiple quorum-sensing pherotypes.* Proceedings of the National Academy of Sciences, 2016. **113**(8): p. 2152-2157.
6. Even-Tov, E., et al., *Transient Duplication-Dependent Divergence and Horizontal Transfer Underlie the Evolutionary Dynamics of Bacterial Cell–Cell Signaling.* PLoS biology, 2016. **14**(12): p. e2000330.
7. Berg, H.C., *Random walks in biology*. 1993: Princeton University Press.
8. Lazazzera, B.A., J.M. Solomon, and A.D. Grossman, *An exported peptide functions intracellularly to contribute to cell density signaling in B. subtilis.* Cell, 1997. **89**(6): p. 917-25.
9. Youk, H. and W.A. Lim, *Secreting and sensing the same molecule allows cells to achieve versatile social behaviors.* Science, 2014. **343**(6171): p. 1242782.
10. Piazza, F., P. Tortosa, and D. Dubnau, *Mutational analysis and membrane topology of ComP, a quorum-sensing histidine kinase of Bacillus subtilis controlling competence development.* Journal of bacteriology, 1999. **181**(15): p. 4540-4548.

11. Schneider, K.B., T.M. Palmer, and A.D. Grossman, *Characterization of comQ and comX, Two Genes Required for Production of ComX Pheromone in Bacillus subtilis.* J. Bacteriol., 2002. **184**(2): p. 410-419.